Manipulation of deep brain activity in primates using transcranial focused ultrasound stimulation

Davide Folloni[1,2*†], Lennart Verhagen[1,2*†], Rogier B. Mars[2,3], Elsa Fouragnan[1,4], Jean-François Aubry[5], Matthew F.S. Rushworth[1,2*], Jérôme Sallet[1,2*†]

[1]Wellcome Centre for Integrative Neuroimaging (WIN), Department of Experimental Psychology, University of Oxford, Oxford, UK

[2]Wellcome Centre for Integrative Neuroimaging (WIN), Centre for Functional MRI of the Brain (FMRIB), Nuffield Department of Clinical Neurosciences, John Radcliffe Hospital, University of Oxford

[3]Donders Institute for Brain, Cognition and Behaviour, Radboud University Nijmegen, Nijmegen, the Netherlands

[4]School of Psychology, University of Plymouth, UK

[5]Institut Langevin, ESPCI ParisTech, CNRS 7587, UMRS 979 INSERM, Paris, France

***Authors contributed equally to the work**

†To whom correspondence should be addressed:

Address: **Davide Folloni, Lennart Verhagen, or Jerome Sallet**

Department of Experimental Psychology,

University of Oxford,

Tinsley Building,

Mansfield Road,

Oxford,

OX1 3SR, UK

E-mail:
davide.folloni@psy.ox.ac.uk
lennart.verhagen@psy.ox.ac.uk
jerome.sallet@psy.ox.ac.uk

Abstract: 69 words

Figures: 3 figures

Abstract

Transcranial focused ultrasound stimulation (TUS) was applied to a deep cortical region, anterior cingulate cortex (ACC, experiment 1) and a subcortical brain structure, the amygdala (experiment 2) in macaques. The impact of TUS was measured by examining functional connectivity patterns between activity in each brain area and in the rest of the brain using functional magnetic resonance imaging (fMRI). Dissociable and spatially focal effects were found in both cases.

To establish the functional role of a brain area it is necessary to examine the impact of disrupting or altering its activity. This can be done reversibly using neuromodulation methods such as transcranial magnetic stimulation and transcranial current stimulation. However, the spatial resolution of these techniques is limited[1,2]. Even more critically, application of these techniques is constrained to the surface of the brain as their efficacy falls off rapidly with depth. An alternative approach, transcranial focused ultrasound stimulation (TUS), has recently been applied[3,4]; when used over the frontal eye field in macaques, TUS leads to latency change during voluntary saccades[5]. Comparatively little, however, is known about TUS's impact on neural activity. We show here that in the macaque (*Macaca mulatta*) TUS transcranially modulates activity with relatively high spatial resolution even in deep cortical regions such as ACC and subcortical nuclei such as the amygdala, and it does so for an extended period after the stimulation and any potential direct acoustic effect has dissipated[6]. An accompanying manuscript reports that TUS to ACC disrupts translation of counterfactual choice values into behavioral change (Fouragnan et al., BioRXiv).

On each day of TUS application, a 40 s train of pulsed ultrasound (250kHz) comprising 30 ms bursts of ultrasound every 100 ms was directed to the target brain region using a single-element transducer in conjunction with a region-specific coupling cone filled with degassed water. Frameless stereotaxic neuronavigation was used to position the transducer over the target brain area taking into consideration the focal depth of the sonication (experiment 1: ACC n=3; experiment 2: amygdala n=4; relatively deep brain regions known to be interconnected and co-active during similar cognitive processes such as social cognition[7,8]; fig.1). A single train was applied to the midline structure, ACC, but one train was applied to each of the more laterally situated amygdalae, in experiments 1 and 2 respectively.

The impact of TUS was determined by examining brain activity over an 80 minute period starting approximately 30 minutes after the 40 s stimulation train began (Supplementary Material). Activity was recorded not just from the stimulated site but from across the entire brain using functional MRI (fMRI). FMRI data from the stimulated animals was compared with data from an additional group of control individuals (n=9) that had received no TUS. FMRI data were acquired at 3T under isoflurane anesthesia and preprocessed using established tools and protocols (Verhagen et al., BioRXiv; Supplementary Material). The anesthesia protocol has previously been shown to preserve regional functional connectivity measurable with fMRI[9].

Although the blood oxygen level dependent (BOLD) signal recorded with fMRI does not provide an absolute measure of activity it does provide a relative measure of activity change in relation to external events or activity recorded from other brain areas. This means that we cannot expect to "see" BOLD changes directly but rather we might find changes in how BOLD responses in one area

relate to BOLD in another area using approaches similar to those employed previously[9]. Following the notion that each brain area is characterized by a unique constellation of projections that determines the role it plays in cognition, we also visualized these coupling patterns in terms of changes in "connectivity fingerprints"[10].

BOLD coupling between brain areas is most prominent when the areas are monosynaptically connected but some residual connectivity is mediated by indirect connections[11]. Accordingly, we found that in control animals ACC activity was coupled with activity in strongly connected areas: dorsal, lateral, and orbital prefrontal cortex (PFC), frontal pole, mid and posterior cingulate (figs.2a,3a). After ACC TUS, however, the ACC coupling pattern was altered (non-parametric permutation test, p=0.0298; fig.2b,3a). A parsimonious interpretation is that normally the activity that arises in ACC is a function of the activity in the areas that project to it but this is no longer the case when ACC's activity is artificially driven or diminished by TUS. Accordingly, altering ACC's relationship with its set of interconnected areas should alter its operation in a specific manner (Fouragnan et al., BioRXiv).

The specificity and selectivity of the effects are underscored by the results observed when 1) stimulating at another location and 2) mapping the coupling pattern of another brain area. First, after TUS over an area anatomically highly connected with the ACC – the amygdala[12], there was minimal change in ACC coupling with other brain areas, beyond its coupling with the amygdala itself and caudal orbitofrontal areas. This suggests ACC-caudal orbitofrontal coupling is mediated by amygdala (figs.2c,3a). Consequentially, amygdala TUS also led to a significant change in ACC connectivity (non-parametric permutation test, p=0.0458) but because the caudal orbitofrontal cortex effect was so circumscribed there was also a significant difference between ACC and amygdala TUS effects (non-parametric permutation test, p=0.0411). Second, when investigating the coupling pattern of a control area with a distinct constellation of projections, such as ventral premotor area F5c, the patterns observed after ACC TUS were virtually indistinguishable from control (fig.S1).

To further examine spatial specificity of TUS effects and to investigate the capacity of TUS to stimulate subcortical structures we also investigated its effects on the coupling of amygdala activity with other brain areas. In controls, amygdala activity is coupled with activity in cingulate, ventral, and orbitofrontal cortex, striatum and the anterior temporal lobe (figs.2d,3b). Activity coupling between the amygdala and all of these areas was reduced after amygdala TUS (non-parametric permutation test, p=0.0016; figs.2f,3b). These effects, however, were not found after ACC TUS, which instead left most of amygdala's coupling pattern unaffected (non-parametric permutation test, p=0.1038; figs.2e,3b) although not surprisingly ACC TUS led to alteration in amygdala's coupling with ACC.

Amygdala TUS also did not affect ACC coupling of a control region (fig.S1). Connectivity changes for regions between the stimulation cone and the targets are also summarized (figs.S2,S3,S4).

In summary, experiments 1 and 2 revealed spatially dissociable effects of ACC and amygdala TUS. The spatially dissociable nature of the effects and the fact that they were observed more than an hour after the 40 s stimulation period suggests they are not mediated by the stimulation's auditory impact[6]. In each case effects were apparent as reductions in activity coupling between the stimulated area and other regions with which it is normally interconnected; after TUS, a brain area's activity appears to be driven less by activity in the areas with which it is connected and more so by the artificial modulation induced by TUS. While the precise mechanism of the impact of TUS on neural activity is being determined[13,14] the current results suggest TUS may be suitable as a tool for focal manipulation of activity in many brain areas in primates.

References

1. Walsh, V. & Cowey, A. *Nat. Rev. Neurosci.* **1,** 73–80 (2000).
2. Dayan, E., Censor, N., Buch, E. R., Sandrini, M. & Cohen, L. G. *Nat. Neurosci.* **16,** 838–844 (2013).
3. Tufail, Y., Yoshihiro, A., Pati, S., Li, M. M. & Tyler, W. J. *Nat. Protoc.* **6,** 1453–1470 (2011).
4. King, R. L., Brown, J. R., Newsome, W. T. & Pauly, K. B. *Ultrasound Med. Biol.* **39,** 312–331 (2013).
5. Deffieux, T. *et al. Curr. Biol.* **23,** 2430–2433 (2013).
6. Sato, T., Shapiro, M. G. & Tsao, D. Y. *Neuron* (2018). doi:10.1016/j.neuron.2018.05.009
7. Munuera, J., Rigotti, M. & Salzman, C. D. *Nat. Neurosci.* **21,** 415–423 (2018).
8. Noonan, M. P. *et al. PLoS Biol.* **12,** e1001940 (2014).
9. Mars, R. B., Sallet, J., Neubert, F.-X. & Rushworth, M. F. S. *Proc. Natl. Acad. Sci.* **110,** 10806–10811 (2013).
10. Passingham, R. E., Stephan, K. E. & Kötter, R. *Nat. Rev. Neurosci.* **3,** 606–616 (2002).
11. O'Reilly, J. X. *et al. Proc. Natl. Acad. Sci. U. S. A.* **110,** 13982–13987 (2013).
12. Amaral, D. G. & Price, J. L. *J. Comp. Neurol.* **230,** 465–496 (1984).

13. Kubanek, J., Shukla, P., Das, A., Baccus, S. A. & Goodman, M. B. *J. Neurosci.* **38,** 3081–3091 (2018).

14. Kubanek, J. *Neurosurg. Focus* **44,** E14 (2018).

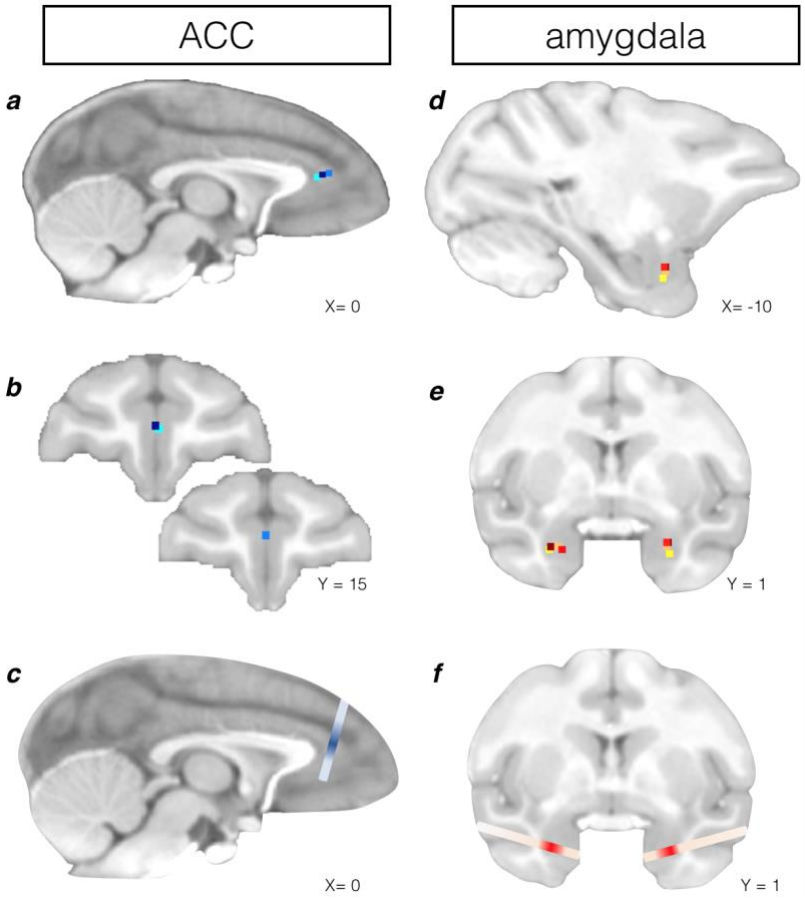

1. Stimulation targets. Stimulation target position is shown for each individual animal (colored dots) on sagittal and coronal views for TUS targeted at ACC (**a-b**) and amygdala (**d**-**e**). The trajectory of stimulation is shown for one example animal per TUS target, ACC (**c**) and amygdala (**f**).

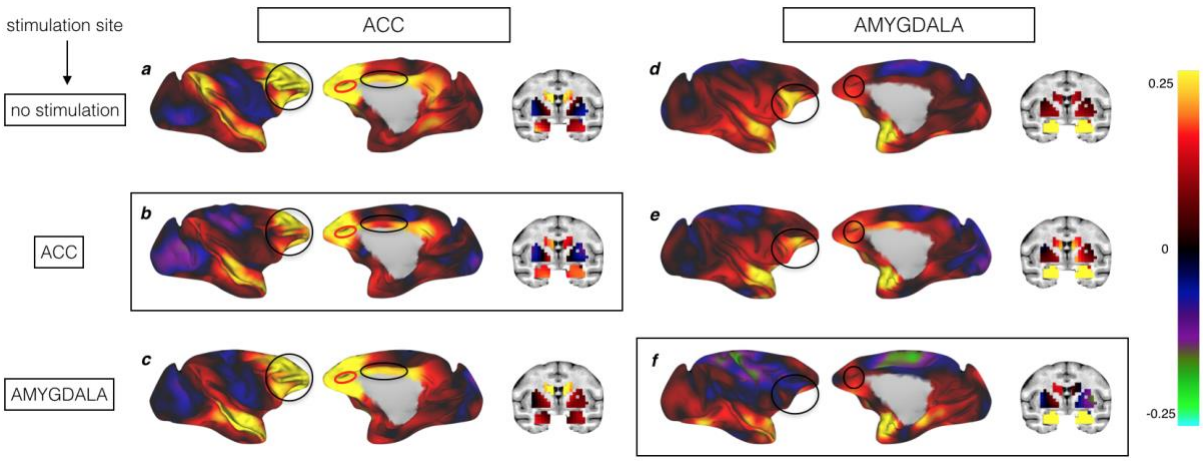

2. Whole-brain functional connectivity between stimulated areas and the rest of the brain. Panels a, b, and c on the left side of the figure show activity coupling between ACC (circled in red) and the rest of the brain in no stimulation/control condition (**a**), after ACC TUS (**b**), and after amygdala TUS (**c**). Panels d, e, f show activity coupling between amygdala (seed masked in yellow) and the rest of the brain in no stimulation/control condition (**d**), after ACC TUS (**e**), and after amygdala TUS (**f**). Hot colors indicate positive coupling (Fisher's z). Functional connectivity from TUS-targeted regions are highlighted by black boxes. Each type of TUS had a selective effect on the stimulated area: ACC coupling was strongly changed by ACC TUS only (b) and amygdala coupling was strongly changed by amygdala TUS only (f). Areas showing changes in coupling with TUS-targeted regions after TUS are circled in black and compared with the other 2 control conditions.

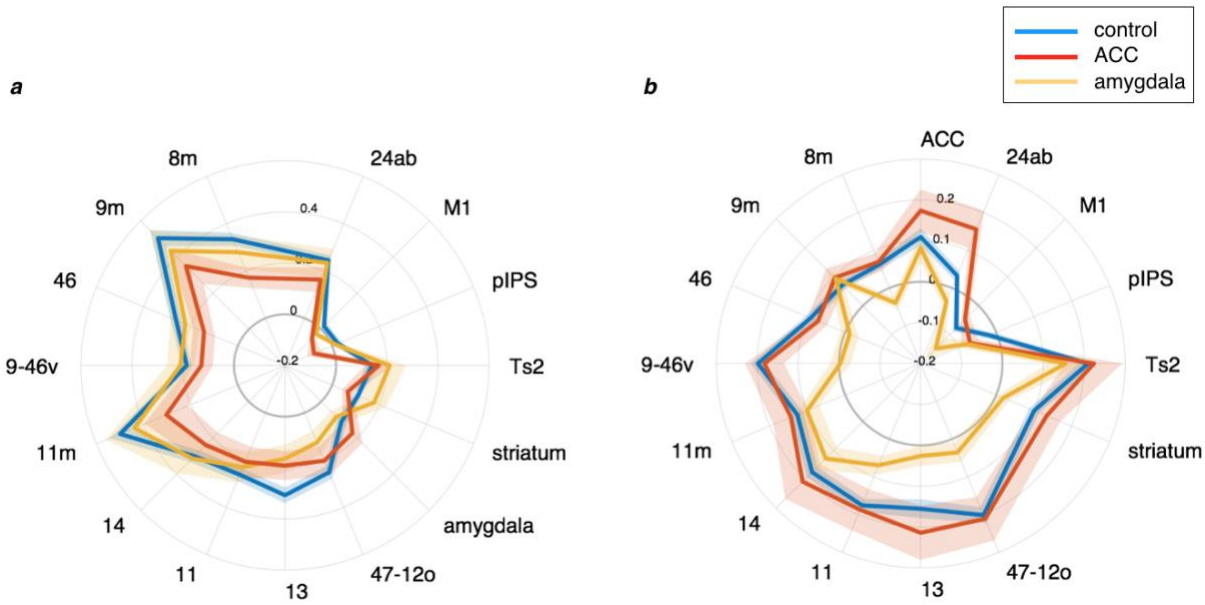

3. ACC and amygdala connectivity fingerprints after stimulation. The lines in the left panel indicates the strength of activity coupling between ACC (**a**) and other brain areas labelled on the circumference in control animals (blue), after ACC TUS (red), and after amygdala TUS (yellow). The lines in the right panel show activity coupling between amygdala (**b**) and the rest of the brain in control animals (blue), after ACC TUS (red), and after amygdala TUS (yellow). Each type of TUS had a selective effect on the stimulated area: ACC coupling was strongly disrupted by ACC TUS (the red line is closer to the center of the panel than the blue line) and amygdala coupling was strongly affected by amygdala TUS (the yellow line is closer to the center of the panel than the blue line). Standard error of the mean is indicated by shading around each line.

Contributions

D.F. and J.S. designed the experiment; D.F. and J.S. collected the data; D.F., L.V., M.F.S.R., and J.S. analyzed the data; L.V. and R.B.M. contributed analysis tools; D.F., L.V., E.F., M.F.S.R., J.F.A., and J.S. wrote the manuscript.

Funding

Funding for this study was provided by a Wellcome Senior Investigator Award (WT100973AIA), MRC programme grant (MR/P024955/1), MRC programme grant (G0902373), Wellcome Trust Henry Dale Fellowship (105651/Z/14/Z), Wellcome Trust UK Grant (105238/Z/14/Z), The Wellcome Centre for Integrative Neuroimaging (203139/Z/16/Z), BBRSC grant (BB/N019814/1), NWO grant (452-13-015), Bettencourt Schueller Foundation and the "Agence Nationale de la Recherche" under the program ‘‘Future Investments’’ (ANR-10-EQPX-15).

METHODS

Ultrasound stimulation

A single-element ultrasound transducer (H115-MR, diameter 64 mm, Sonic Concept, Bothell, WA, USA) with a 51.74 mm focal depth was used with region-specific coupling cones filled with degassed water and sealed with a latex membrane (Durex) to assess TUS of ACC (experiment 1; n=3) and amygdala (experiment 2; n=4) (fig.1). The ultrasound wave frequency was set to the 250 kHz resonance frequency and 30 ms bursts of ultrasound were generated every 100 ms with a digital function generator (Handyscope HS5, TiePie engineering, Sneek, the Netherlands). Overall, the stimulation lasted for 40 s. A 75-Watt amplifier (75A250A, Amplifier Research, Souderton, PA) was used to deliver the required power to the transducer. A TiePie probe (Handyscope HS5, TiePie engineering, Sneek, The Netherlands) connected to an oscilloscope was used to monitor the voltage delivered. The recorded peak-to-peak voltage was constantly maintained at 130V and corresponded to a peak negative pressure of 1.2MPa measured in water with an in-house heterodyne interferometer[1]. Based on a mean 66% transmission through the skull[2], the estimated peak negative pressures applied are of 0.84 MPa at the target in the brain. A single train was applied to the midline structure (ACC) but one train was applied to each of the more laterally situated amygdalae in experiments 1 and 2 respectively.

Each individual animal's structural magnetic resonance (MRI) image was registered to its head with a frameless stereotaxic neuronavigation system (Rogue Research, Montreal, CA). By recording the positions of both the ultrasound transducer and the head with an infrared tracker it was then possible to co-register the ultrasound transducer with respect to the MRI scan of the brain to position the transducer over the targeted brain region, either ACC[3] (MNI coordinates x = 0, y = 15, z = 6) or amygdala (MNI coordinates x = -10, y = 1, z = -11; x = 9, y = 1, z =11). The ultrasound transducer / coupling cone montage was placed directly onto previously shaved skin on which conductive gel (SignaGel Electrode; Parker Laboratories Inc.) had been applied to ensure ultrasonic coupling between the transducer and the animal's head. In the non-stimulation condition (control), all procedures (anaesthesia, pre-scan preparation, fMRI scan acquisition and timing), with the exception of actual TUS, mirrored the TUS sessions.

Macaque rs-fMRI Data Acquisition, Preprocessing, and Analysis.

Resting state fMRI (rs-fMRI) and anatomical MRI scans were collected for 11 healthy macaques (*Macaca mulatta*) (two females; rs-fMRI from nine animals were acquired under no stimulation; rs-fMRI from three animals were acquired post ACC TUS; rs-fMRI from four animals were acquired post amygdala TUS; age: 7.3 years, weight: 10.3 kg) under inhalational isoflurane anesthesia using a

protocol which was previously proven successful[4,5] in preserving whole-brain functional connectivity as measured with BOLD signal. In the case of the TUS conditions, fMRI data collection began only after completion of the TUS train (delay between ultrasound stimulation offset and scanning onset: 37.5 minutes; SEM: 2.21 minutes). Anesthesia was induced using intramuscular injection of ketamine (10 mg/kg), xylazine (0.125– 0.25 mg/kg), and midazolam (0.1 mg/kg). Macaques also received injections of atropine (0.05 mg/kg, intramuscularly), meloxicam (0.2 mg/kg, intravenously), and ranitidine (0.05 mg/kg, intravenously). To block peripheral nerve stimulation, 15 minutes before placing the macaque in the stereotaxic frame local anaesthetic (5% lidocaine/prilocaine cream and 2.5% bupivacaine) was also administered via subcutaneous injection around the ears. The anesthetized animals were placed in an MRI-compatible stereotactic frame (Crist Instruments) in a sphinx position and placed in a horizontal 3 T MRI scanner with a full-size bore. Scanning commenced 1.53 hours (SEM: 4 minutes) and 2.38 hours (SEM: 4 minutes) after anesthesia induction in TUS and control sessions, respectively. In both cases data collection commenced when the clinical peak of ketamine had passed. Anesthesia was maintained, in accordance with veterinary recommendation, using the lowest possible concentration of isoflurane to ensure that macaques were anesthetized. The depth of anesthesia was assessed and monitored using physiological parameters (heart rate and blood pressure, as well as clinical checks before the scan for muscle relaxation). During the acquisition of the functional data, the inspired isoflurane concentration was in the range 0.8–1.1%, and the expired isoflurane concentration was in the range 0.7-1%. Isoflurane was selected for the scans as it was previously demonstrated to preserve rs-fMRI networks[5,6,7]. Macaques were maintained with intermittent positive pressure ventilation to ensure a constant respiration rate during the functional scan, and respiration rate, inspired and expired CO2, and inspired and expired isoflurane concentration were monitored and recorded using VitalMonitor software (Vetronic Services Ltd.). Core temperature and SpO2 were also constantly monitored throughout the scan.

A four-channel phased-array coil was used for data acquisition (Dr. H. Kolster, Windmiller Kolster Scientific, Fresno, CA, USA). Whole-brain BOLD fMRI data were collected from each animal for up to 78 minutes. All fMRI data were collected using the following parameters: 36 axial slices; in-plane resolution, 2 x 2 mm; slice thickness, 2 mm; no slice gap; TR, 2000 ms; TE, 19 ms; 800 volumes per run. A minimum period of 10 days elapsed between sessions.

A structural scan (average over up to three T1-weighted structural MRI images) was acquired for each macaque in the same session as the functional scans, using a T1-weighted magnetization-prepared rapid- acquisition gradient echo sequence (0.5 x 0.5 x 0.5 mm voxel resolution).

All recording and stimulation procedures were conducted under licenses from the United Kingdom (UK) Home Office in accordance with The Animals (Scientific Procedures) Act 1986 and with the European Union guidelines (EU Directive 2010/63/EU).

The preprocessing and analysis of the MRI data was designed to follow the HCP Minimal Processing Pipeline[8], using tools of FSL (https://fsl.fmrib.ox.ac.uk/fsl/fslwiki), HCP Workbench (https://www.humanconnectome.org/software/connectome-workbench), and the Magnetic Resonance Comparative Anatomy Toolbox (MrCat; www.neuroecologylab.org). The processing pipeline has been validated and described in full (Verhagen et al., BioRxiv).

The T1w images were processed in an iterative fashion cycling through brain-extraction (BET)[9], RF bias-field correction, and linear and non-linear registration (FLIRT and FNIRT)[10,11] to the macaca mulatta F99 atlas[12,13]. The application of robust and macaque-optimised versions of BET and FAST[14] also provided segmentation into grey matter, white matter, and cerebral spinal fluid compartments. Segmentation of subcortical structures was obtained by registration to the D99 atlas[15].

The first 5 volumes of the functional EPI datasets were discarded to ensure a steady RF excitation state. EPI timeseries were motion corrected using MCFLIRT. Given that the animals were anesthetized and their heads were held in a steady position, any apparent image motion, if present at all, is caused by changes to the B0 field, rather than by head motion. Accordingly, the parameter estimates from MCFLIRT can be considered to be 'B0-confound parameters' instead. Each timeseries was checked rigorously for spikes and other artefacts, both visually and using automated algorithms; where applicable slices with spikes were linearly interpolated based on temporally neighboring slices. Brain extraction, bias-correction, and registration was achieved for the functional EPI datasets in an iterative manner, similar to the preprocessing of the structural images with the only difference that the mean of each functional dataset was registered to its corresponding T1w image using rigid-body boundary-based registration (FLIRT). EPI signal noise was reduced both in the frequency and temporal domain. First, the functional time series were high-pass filtered at 2000s. Temporally cyclical noise, for example originating from the respiratory apparatus, was removed using band-stop filters set dynamically to noise peaks in the frequency domain. Remaining temporal noise was described by the mean time course and first two subsequent principal components of the white matter (WM) and cerebral spinal fluid (CSF) compartment (considering only voxels with a high posterior probability of belonging to the WM or CSF, obtained in the T1w image using FAST). The B0-confound parameter estimates were expanded as a second degree Volterra series to capture both linear and non-linear B0 effects. Together the WM and CSF expanded B0 confound parameters were regressed out of the BOLD signal for each voxel.

The cleaned time course was then low-pass filtered with a cut-off at 10 seconds. The cleaned and filtered signal was projected from the conventional volumetric representation (2mm voxels) to the F99 cortical surface (~1.4mm spaced vertices) using Workbench command "myelin-style" mapping, while maintaining the subcortical volumetric structures. The data was spatially smoothed using a 3mm FWHM gaussian kernel, while taking into account the folding of the cortex and the anatomical boundaries of the subcortical structures. Lastly, the data were demeaned to prepare for functional connectivity analyses.

To represent subject effects, the timeseries from the three runs were concatenated to create a single timeseries per animal per intervention (control, ACC TUS, amygdala TUS). To represent group effects the run-concatenated timeseries of all animals were combined using a group-PCA approach[16] that was set to reduce the dimensionality of the data.

To construct a region-of-interest (ROI) for ACC, a circle of 4mm radius was drawn on the cortical surface around the point closest to the average stimulation coordinate (fig.1), in both the left and the right hemisphere. The same procedure was used to define other bilateral cortical regions of interest, based on literature coordinates[5,17,18], to serve as targets for the fingerprint analyses (fig.3).

Coupling between the activity of each region of interest and the rest of the brain was estimated by calculating the Fisher's z-transformed correlation coefficient between each point in the ROI and all other datapoints. The resulting "connectivity-maps" were averaged across all points in the ROI, across both hemispheres. Accordingly, the final maps represent the average coupling of a bilateral ROI with the rest of the brain. The fingerprints are obtained by extracting the average coupling with each target ROI and averaging across the two hemispheres. Statistical inference on the fingerprints was performed by using non-parametric permutation tests on cosine similarity metrics describing how similar or dissimilar pairs of fingerprints are[19] (Verhagen et al., BioRxiv). In contrast to conventional parametric tests, this approach does not rely on assumptions about the shape of the distribution but will acknowledge dependencies between target ROIs in the fingerprint; as such this approach will avoid inflation of type I error. For each test we ran 10,000 permutations to accurately approximate the true probability of rejecting the null-hypothesis of permutable conditions.

References

1. Constans, C., Deffieux, T., Pouget, P., Tanter, M. & Aubry, J.-F. *IEEE Trans. Ultrason. Ferroelectr. Freq. Control* **64,** 717–724 (2017).
2. Wattiez, N. *et al. Brain Stimulat.* **10,** 1024–1031 (2017).
3. Procyk, E. *et al. Cereb. Cortex N. Y. NY* **26,** 467–476 (2016).

4. Noonan, M. P. *et al. PLoS Biol.* **12,** e1001940 (2014).

5. Neubert, F.-X., Mars, R. B., Sallet, J. & Rushworth, M. F. S. *Proc. Natl. Acad. Sci.* **112,** E2695–E2704 (2015).

6. Mars, R. B., Sallet, J., Neubert, F.-X. & Rushworth, M. F. S. *Proc. Natl. Acad. Sci.* **110,** 10806–10811 (2013).

7. Vincent, J. L. *et al. Nature* **447,** 83–86 (2007).

8. Glasser, M. F. *et al. NeuroImage* **80,** 105–124 (2013).

9. Smith, S. M. *Hum. Brain Mapp.* **17,** 143–155 (2002).

10. Jenkinson, M. & Smith, S. *Med. Image Anal.* **5,** 143–156 (2001).

11. Jenkinson, M., Bannister, P., Brady, M. & Smith, S. *NeuroImage* **17,** 825–841 (2002).

12. Van Essen, D. C. *Ann. N. Y. Acad. Sci.* **978,** 468–479 (2002).

13. Van Essen, D. C. & Dierker, D. L. *Neuron* **56,** 209–225 (2007).

14. Zhang, Y., Brady, M. & Smith, S. *IEEE Trans. Med. Imaging* **20,** 45–57 (2001).

15. Reveley, C. *et al. Cereb. Cortex N. Y. N 1991* **27,** 4463–4477 (2017).

16. Smith, S. M., Hyvärinen, A., Varoquaux, G., Miller, K. L. & Beckmann, C. F. *NeuroImage* **101,** 738–749 (2014).

17. Sallet, J. *et al. J. Neurosci. Off. J. Soc. Neurosci.* **33,** 12255–12274 (2013).

18. Neubert, F.-X., Mars, R. B., Thomas, A. G., Sallet, J. & Rushworth, M. F. S. *Neuron* **81,** 700–713 (2014).

19. Mars, R. B. *et al. Neurosci. Biobehav. Rev.* **60,** 90–97 (2016).

20. Hoesen, G. W. V., Morecraft, R. J. & Vogt, B. A. *Neurobiology of Cingulate Cortex and Limbic Thalamus* 249–284 (Birkhäuser, Boston, MA, 1993). doi:10.1007/978-1-4899-6704-6_9

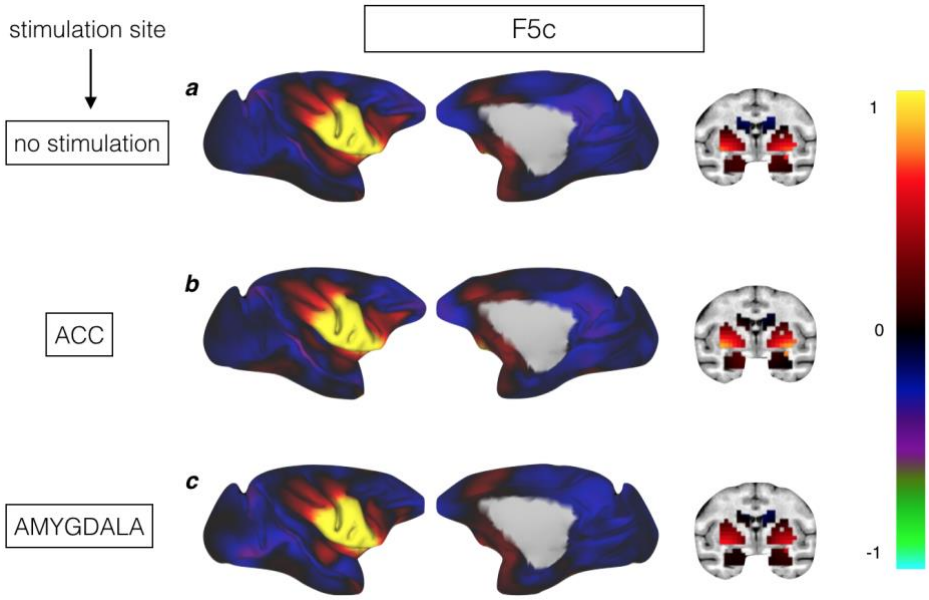

Supplementary figure 1. Whole-brain functional connectivity between stimulated and not stimulated areas with the rest of the brain. Panels a, b, and c show activity coupling between a control area, the caudal ventral premotor area F5c, and the rest of the brain in no stimulation/control condition (**a**), after ACC TUS (**b**), and after amygdala TUS (**c**). Hot colors indicate positive coupling (Fisher's z). Compared to a no stimulation condition (a), neither ACC TUS nor amygdala TUS (b,c) affected the whole-brain coupling activity of F5c which has weak anatomical connections with ACC and amygdala.

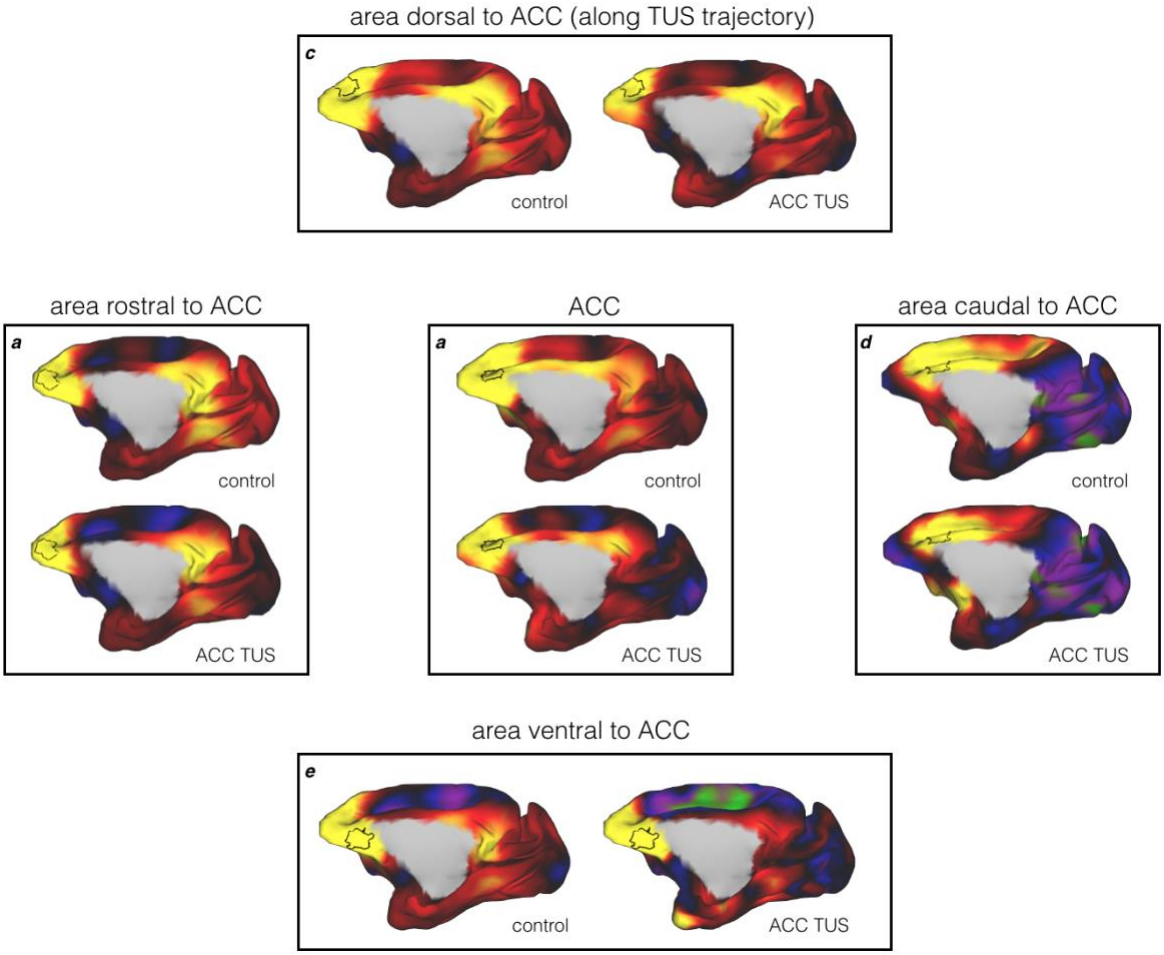

Supplementary figure 2. Whole-brain activity coupling of the areas neighboring ACC in the control condition and after ACC TUS. (**a, central panel**) As also shown in figure 2, the whole brain coupling of the ACC target region (black outline) is significantly different in the control condition and when TUS is applied to ACC. Panels b, c, d and e show the activity coupling of regions near the ACC target in both the ACC TUS and control conditions. This includes areas located along the trajectory of the ultrasound stimulation beam such as (**c**) the area in between the transducer and the target region in ACC (again indicated by black outline) and the area on the other side of the target region (**e**) as well as areas immediately anterior (**b**) and posterior(**d**) to the target region. Minimal changes in coupling of each region and the rest of the brain can be seen along the stimulation trajectory (**c**,**e**) but some alteration can be seen in areas which are not hit by the ultrasound beam (**b**,**d**). For example, these post-stimulation changes are visible in the area most immediately posterior to ACC (**d**). This area is strongly anatomically connected with the targeted area[20]. These results reinforce the spatial specificity of TUS and suggest that if its effect spread then the spread is mediated by anatomical connections rather than spatial proximity to ultrasound beam. Further evidence that spread is mediated by anatomical connections rather than due to spatial proximity is shown in fig.S4 below.

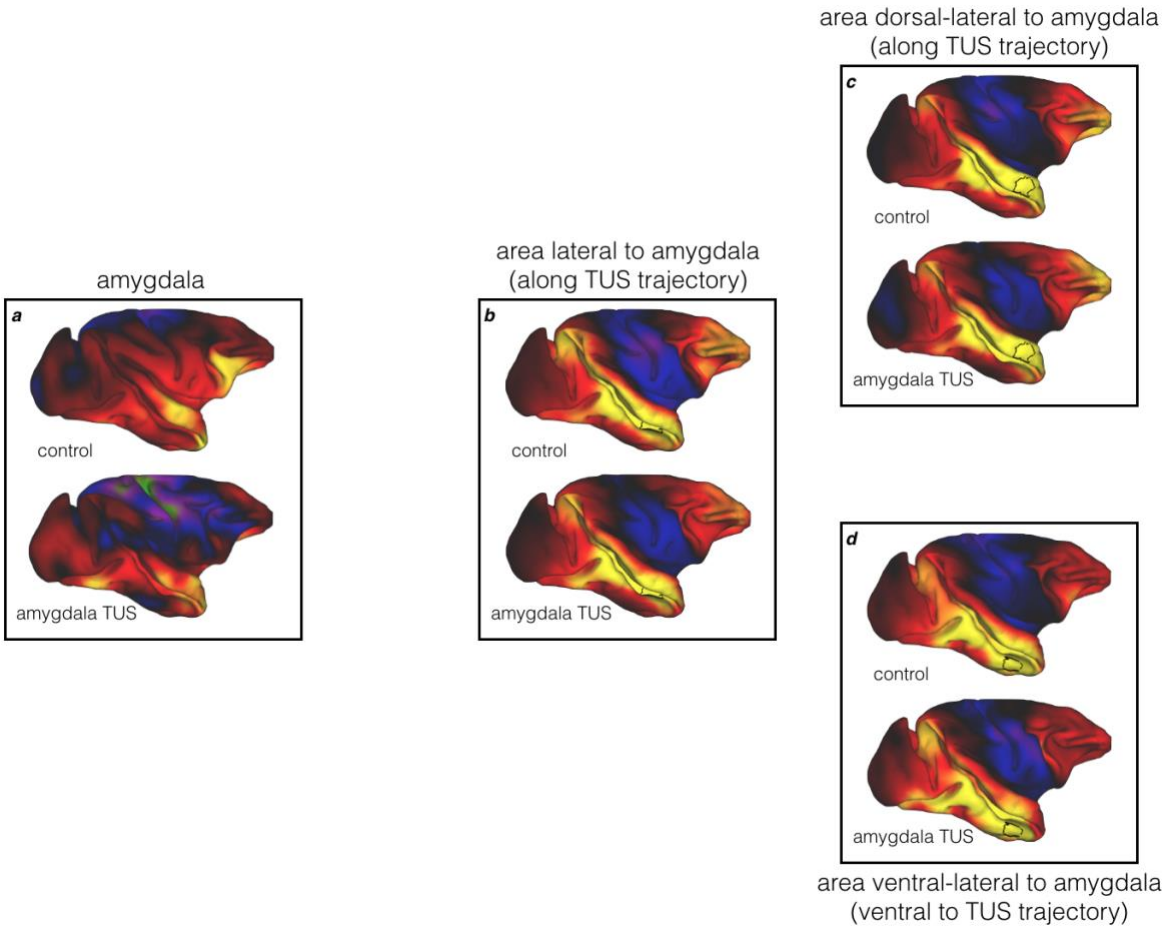

Supplementary figure 3. Whole-brain activity coupling of areas neighboring amygdala after amygdala TUS and in the control condition. (**a**) As also shown in figure 3, the whole-brain coupling of the amygdala target region is significantly different in the control condition and when TUS is applied to the amygdala. Panels b, c, d show the activity coupling of regions along (**b**,**c**) or immediately surrounding the trajectory of the ultrasound stimulation beam (**d**, the outline in black in all cases indicates the regions for which the whole-brain connectivity is shown) in the control condition and after amygdala TUS. As with the analogous results after ACC TUS (fig.S2), there were no changes in the coupling of these regions and the rest of the brain. This is true for the regions through which the stimulation trajectory passed in the fundus of the superior temporal sulcus (**b**) and the superior temporal gyrus (**c**) or in the immediately adjacent inferior temporal gyrus (**d**). This lack of major changes after amygdala TUS was also found in seven other regions investigated in the anterior temporal lobe (not shown).

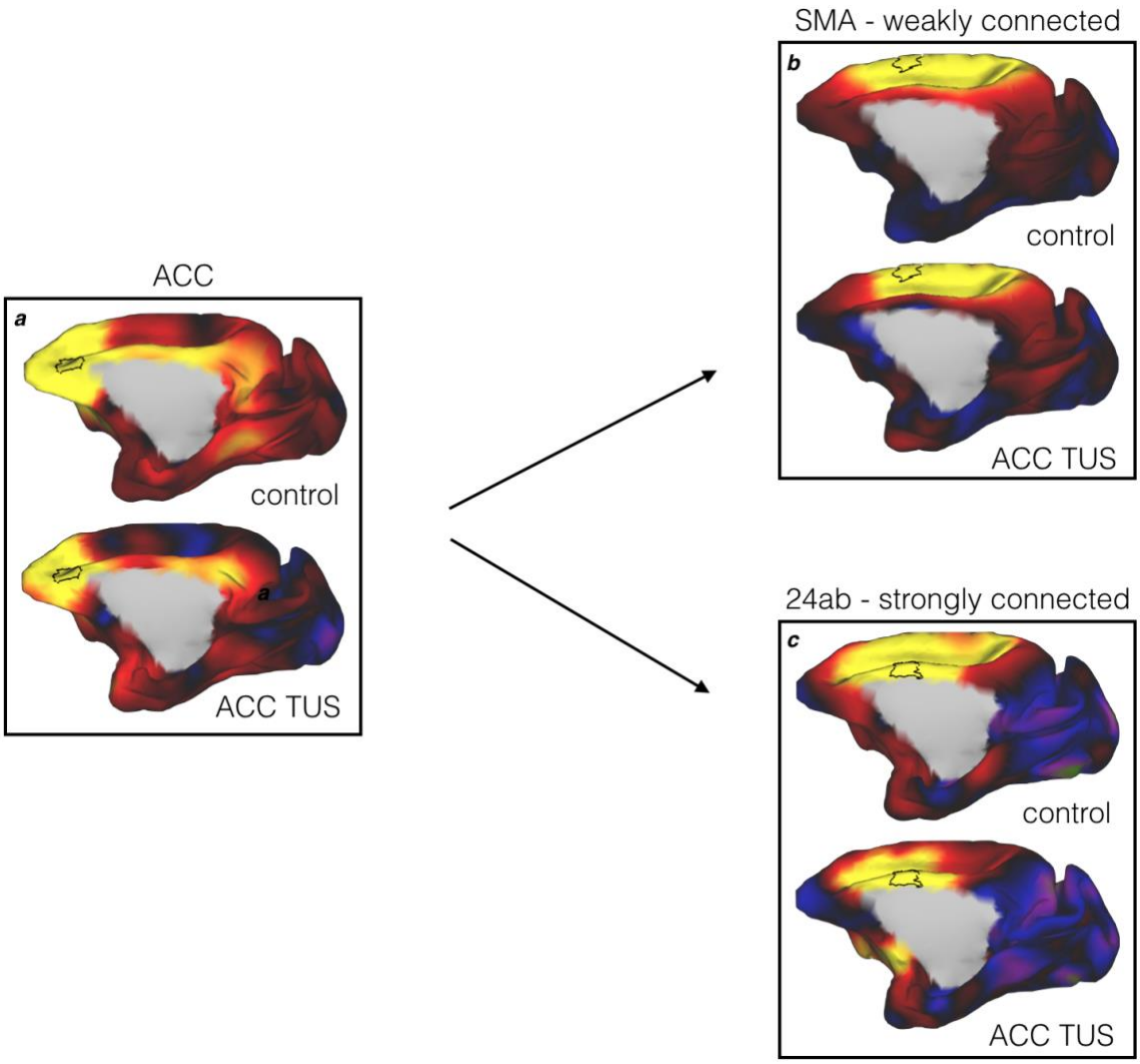

Supplementary figure 4. **Effects of TUS on regions outside the target area are mediated by the strength of anatomical connectivity rather than a result of spatial proximity.** Panels a, b, and c of the figure show whole-brain activity coupling in control and ACC TUS conditions for ACC (**a**) and two areas at an equal Euclidian distance from the ACC target region: SMA (**b**) and area 24ab (**c**). Hot colors indicate positive coupling (Fisher's z). The activity coupling of SMA, an area weakly connected with the target area ACC, and the rest of the brain is predominantly preserved after TUS. However, the whole-brain coupling of an area more strongly connected with the target ACC region[20], area 24b, is more influenced by TUS to the ACC target region.